



New Perspectives on Foot Segment Forces and Joint Kinetics—Integrating Plantar Shear Stresses and Pressures with Multi-segment Foot Modeling

Dustin A. Bruening¹ · Spencer R. Petersen¹ · Sarah T. Ridge²

Received: 9 November 2022 / Accepted: 24 February 2024 / Published online: 17 March 2024
© The Author(s) under exclusive licence to Biomedical Engineering Society 2024

Abstract

The role of the many small foot articulations and plantar tissues in gait is not well understood. While kinematic multi-segment foot models have increased our knowledge of foot segmental motions, the integration of kinetics with these models could further advance our understanding of foot mechanics and energetics. However, capturing and effectively utilizing segmental ground reaction forces remains challenging. The purposes of this study were to (1) develop methodology to integrate plantar pressures and shear stresses with a multi-segment foot model, and (2) generate and concisely display key normative data from this combined system. Twenty-six young healthy adults walked barefoot (1.3 m/s) across a pressure/shear sensor with markers matching a published 4-segment foot model. A novel anatomical/geometric template-based masking method was developed that successfully separated regions aligned with model segmentation. Directional shear force plots were created to summarize complex plantar shear distributions, showing opposing shear forces both between and within segments. Segment centers of pressure (CoPs) were shown to be primarily stationary within each segment, suggesting that forward progression in healthy gait arises primarily from redistributing weight across relatively fixed contact points as opposed to CoP movement within a segment. Inverse dynamics-based normative foot joint moments and power were presented in the context of these CoPs to aid in interpretation of tissue stresses. Overall, this work represents a successful integration of motion capture with direct plantar pressure and shear measurements for multi-segment foot kinetics. The presented tools are versatile enough to be used with other models and contexts, while the presented normative database may be useful as a baseline comparison for clinical work in gait energetics and efficiency, balance, and motor control. We hope that this work will aid in the advancement and availability of kinetic MSF modeling, increase our knowledge of foot mechanics, and eventually lead to improved clinical diagnosis, rehabilitation, and treatment.

Keywords Instrumented gait analysis · Force partitioning · Center of pressure · Foot energetics · Footprint mask · Anatomical masking · Geometric masking · Butterfly or Pedotti diagram

Abbreviations

GRF Ground reaction force
MSF Multi-segment foot
CoP Center of pressure
AP Anterior/posterior

ML Medial/lateral
1MTP 1st metatarsophalangeal (joint)
23MTP Joint between 2nd and 3rd metatarsophalangeal joints
ROI Region of interest
BW Body weight
MLA Medial longitudinal arch

Associate Editor Michael R. Torry oversaw the review of this article.

✉ Dustin A. Bruening
dabruening@byu.edu

¹ Department of Exercise Sciences, Brigham Young University, 120F RB, Provo, UT 84602, USA

² Department of Rehabilitation Sciences, University of Hartford, West Hartford, CT 06117, USA

Introduction

With advancing technological capabilities, the field of human movement science has gradually expanded to focus greater attention on the role of smaller, more complex structures such as the foot. The foot's interaction with the ground

during locomotion is typically captured as ground reaction forces (GRFs) or plantar pressure distributions from force plates or pressure mats. Additional insights are gleaned when foot forces are combined with motion capture-based models of the lower limbs, leading, for example, to inverse dynamics derived joint kinetics or individual muscle force estimates from musculoskeletal simulations. Traditionally, these integrated models have treated the foot as a single rigid segment; however, their expansion to include segments and joints within the foot is an emerging and extremely challenging area of exploration [1–4]. Overcoming some of the technological hurdles impeding progress in this area could be extremely rewarding, leading to increased understanding of the foot's role in gait energetics and increasing our ability to treat pathologies.

Multi-segment foot (MSF) models have increasingly been used to measure foot segment motion; however, technical challenges have limited the integration of kinetics to these efforts. Numerous kinematic MSF models have been published, either as stand-alone papers or as part of application research [5]. While segment reference frames have been useful in quantifying foot joint motion, they are limited in capturing tissue mechanics. Several attempts at integrated kinematic and kinetic models have been presented; however, a hurdle in measuring segmental GRFs has persisted [6, 7]. Strain gauge or piezoelectric-based force platforms return only a single net GRF vector, center of pressure (CoP), and free moment. Resistance and capacitance-based pressure mats, on the other hand, provide full plantar pressure distributions and segmental CoPs, but do not capture shear forces. Both methods are commonly used in instrumented gait analysis, albeit separately. A few previous attempts have been made at capturing full subarea GRFs through the use of multiple adjacent force platforms [1, 4] or force partitioning either from a single force platform [8] or by overlaying and integrating a pressure mat on top of a force platform [3, 9–11]. All of these methods have relied on assumptions about the manner in which parts of the GRFs are distributed under the foot [7].

Recent advances in shear sensing technology now allow for direct measurement of plantar shear stresses and full subarea GRF distributions [12]; however, their integration with motion capture-based modeling presents several hurdles. This technology has been used to measure plantar shear stress distributions in pathologies such as diabetes [13, 14], but has not yet been integrated with motion capture and MSF modeling. Such integration requires not only temporal and spatial synchronization between the two systems, but also modeling alignment. For instance, subarea forces need to be segmented, or “masked”, in a manner consistent with MSF segment definitions so that the forces can be used as inputs to the model. Masking using composite plantar pressure footprints is a common process, but is typically performed using only the geometry of the footprint

itself (i.e., geometric masking) [15, 16]. A few studies have integrated motion capture with plantar pressure, masking the foot regions of the plantar pressure footprint using markers from a MSF model (i.e., anatomical masking) [17–20]. However, this methodology has to date focused only on leveraging landmark locations, and the resulting masked regions do not correspond to the segments of the MSF model.

Data generated from this type of multi-faceted and integrated system could increase our understanding of foot mechanics when effectively analyzed. For example, normative data increases our understanding of healthy gait mechanics and serves as a baseline or comparison for pathological gait [21]. Presenting this data in useful ways is an ongoing challenge [22] that is further complicated with the addition of full plantar pressure and shear measurements, exacerbating already existing challenges in data handling and reporting. For instance, due its already large data format, plantar pressures have almost exclusively been presented as metrics, such as peaks, gradients, or pressure-time integrals, broken into geometrically masked foot regions. For GRFs and model-based measures of joint angles, moments, and powers, metrics have also traditionally been extracted to make comparisons (e.g., peaks, integral, mean, etc.), although newer waveform analysis is becoming more common [23]. Other more complex plots (e.g., Pedotti diagrams) can also be useful for visualization of individual participants. The expansive data generated by combining pressure and shear measurements with motion capture require additional techniques to analyze and report key information in order to be useful in clinical applications.

The purposes of this study were twofold: (1) to develop methodology to integrate plantar pressure and shear stress measurements with MSF modeling and inverse dynamics, and (2) to generate and effectively present normative data from this system. Specifically for the first purpose, we focused on automation, hypothesizing that segment masks that matched MSF segmentation could be accurately automated using a combination of geometric and anatomical masking techniques. For the second purpose, we hypothesized that opposing GRFs would be present both within and between segments [6, 13, 14] and could be displayed in a concise manner [14, 24]. In addition, we hypothesized that segmental CoPs would be largely confined to specific identifiable locations within the segment. If true, static CoP locations could provide a simple framework for interpreting foot joint moments, expanding the use of underutilized frontal and transverse plane moments.

Materials and Methods

Participants

Twenty-six young healthy adults participated (15 m, 11 f; age: 26.6 ± 7.5 ; height: 180.1 ± 5.0 cm; mass = 81.5 ± 8.8 kg,

all racially white). All were free from current injury or any condition that might affect typical walking patterns. All participants were volunteers and signed consent forms approved by the local ethics board (Protocol X2019-383).

Equipment and Protocol

Twenty-one retroreflective markers were adhered to each participants' left leg and foot according to a custom kinetic multi-segment foot model. Full marker placement and model details are described in Williams et al. [25] (and based on earlier work [1, 26]), with one modification. Briefly, the previous model defines shank, rearfoot, mid/forefoot, and hallux segments separated by ankle, midtarsal, and first metatarsophalangeal (1MTP) joints, respectively. For this study, we added a lateral toes segment with a joint between the 2nd and 3rd metatarsal heads (23MTP). This segment did not contain any markers, thus its motion was simply matched to the motion of the hallux.

Following marker placement and a static pose collection, participants walked across a 5.5 m long raised walkway containing a commercial shear/pressure sensor (FootSTEPS, ISSI, Dayton, OH, USA) (Fig. 1). The device consists of a surface stress sensitive film on a glass substrate, a camera below the glass, and a force platform (AMTI, Watertown MA, USA) for calibration. As participants walk across the sensing area (0.43 m by 0.28 m), film displacements are optically measured by the camera. Initial processing includes converting these displacements to vertical pressure, medialateral (ML) shear stress, and anteroposterior (AP) shear stress using a finite element reconstruction model. Note that ML and AP forces are presented with reference to the foot (as opposed to the sensor). Details regarding this device hardware, measurement validity, and initial processing have been previously presented [12]. For this study, images were sampled at 50 Hz, while the force platform was sampled

at 1000 Hz. Motion data were sampled at 100 Hz with a 12-camera motion capture system (Qualisys, Gottberg, Sweden).

Walking speed was controlled at 1.3 m/s and monitored with timing lights (Bower, Draper UT USA). Participant starting position was adjusted to prevent targeted foot placement. Three trials with successful speed (± 0.02 m/s) and foot placement were collected for analysis.

Data Processing

Initial processing was performed using custom algorithms written in LabView software (NI, Austin, TX, USA). This included four main steps: 1- Synchronization, 2- Segment Masking, 3- Dynamic Pressure Scaling, and 4- GRF Construction. Final segmental force data were then imported into commercial software for full MSF modeling and inverse dynamics.

Synchronization

Temporal synchronization was accomplished during collection using a hardware trigger from the motion capture system to the digital force platform amplifier. The motion capture system was then manually started and the time delay between it and the automatic capture of pressure/shear (upon a threshold of 10 N) was recorded and used as an automated time shift in the custom software. Force platform data were then downsampled from 1000 to 100 Hz while pressure and shear data were upsampled from 50 to 100 Hz.

Spatial registration was accomplished by rotationally aligning the motion capture calibration reference frame with the FootSTEPS sensing area, so that only an origin offset was required to register the two reference frames. This offset was determined by pressing a digitizing pointer, with known motion capture coordinates, onto the surface, and calculating

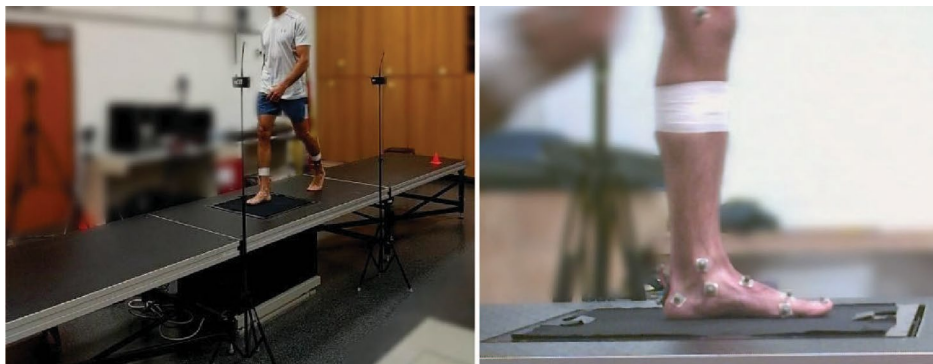


Fig. 1 Experimental Setup. Left panel shows a participant on the walkway while the right panel is a close up of the foot showing the markers and device surface. The 5.5 m length walkway was created from adjustable height staging panels. A hole was cut in the center

panel for the pressure/shear sensor and a small (< 1 cm) gap was maintained around the device perimeter. Timing lights used to monitor walking speed are also visible

the average offset between the pointer tip in both reference frames.

Segment Masking

A composite footprint was created by extracting the peak pressure at each pixel location. Marker positions were identified at their instance of minimum velocity (in mid-stance) and projected downward onto the pressure footprint. Four regions that matched the MSF model segment definitions were then masked using a process that combined anatomical and geometric techniques (Fig. 2). First, a manual template was constructed from one sample training footprint. The division between rearfoot and mid/forefoot was a straight line between markers on the navicular and cuboid bones, passing through themidtarsal joint center. Divisions separating forefoot, hallux, and lateral toe regions were based on footprint geometry, with lines drawn where pressure was minimized. Next, the drawn points for each region of interest (ROI) in the training footprint were calculated as barycentric coordinates, expressed relative to segment-specific triangles created from the anatomical markers

(Fig. 2A). These barycentric coordinates were saved as a master template, then applied to the other footprints, reconstructing initial masks based on the locations of the markers (Fig. 2B). Finally, the lines around the distal segments were adjusted using a simple implementation of a gradient descent optimization routine: distal edge ROI points were iteratively adjusted anteriorly/posteriorly until the pressure was either zero or the gradient changed directions (i.e., at a minimum). Similarly, the ROI points between the hallux and lateral toes were adjusted medially/laterally in the same manner (Fig. 2C).

Dynamic Pressure Scaling

The film properties inherently capture shear stress magnitudes more accurately than vertical pressure magnitudes; however, the force platform provides a gold standard reference for the total vertical force, thus this was used to dynamically scale the reconstructed pressure values as suggested by Goss et al. [12] This was done by simply scaling the total force from the film to the force platform at each time frame. The ratio of the film force to platform force was used as a

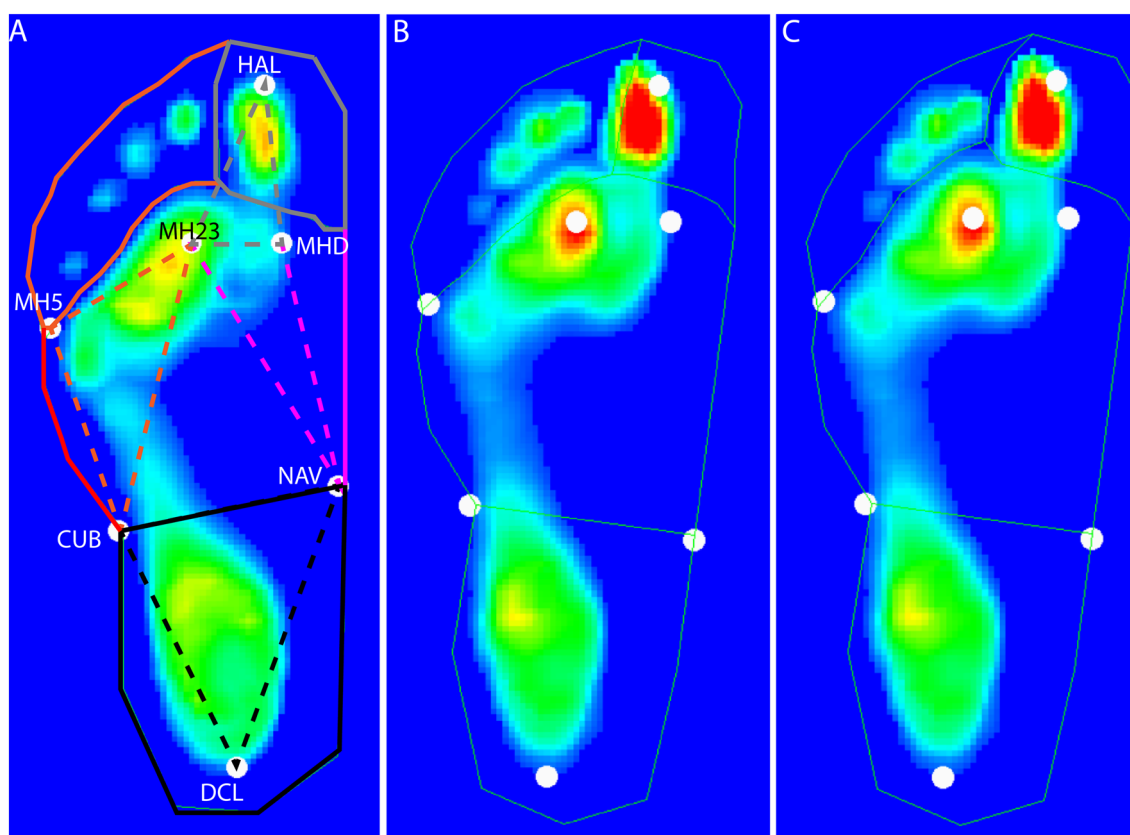


Fig. 2 Segment masking process. **A** A template (solid lines) was first created manually on one footprint and expressed as barycentric coordinates relative to specific triangles (dashed lines) formed by the motion capture markers (white circles). The boundary points associ-

ated with each triangle are shown in different colors. **B** The template was then applied to a new footprint. **C** The forefoot and toe boundary lines were adjusted using gradient descent

scale factor, which was then applied to all pixels of the pressure image (this by necessity assumes that the relative pressure is accurate, a common assumption in other pressure-based measurement systems). Dynamic pressure scaling was performed after segment masking so that all spurious data could be removed by setting to zero all pressure data outside of the masked regions.

Segmental GRF Construction

Net GRF profiles were calculated for each segment, consisting of force, center of pressure, and free moment, expressed in the lab reference frame ($X \approx$ AP, $Y \approx$ ML, $Z =$ Vertical). Segment forces along each axis were calculated as the sum of the products of pixel pressure (P_i) or shear stress (σ_i) and the square area of the pixel (A_i) (Eq. 1). The center of pressure (CoP_{seg}) was calculated as the weighted average of pixel locations in AP and ML directions (Eq. 2). The free moment (M_{seg}) was calculated as the sum of the shear force moments about the center of pressure (vector cross product, $R \times F$) (Eq. 3).

$$F_{Zseg} = \Sigma(P_i A_i) \quad F_{Xseg} = \Sigma(\sigma_{X_i} A_i) \quad F_{Yseg} = \Sigma(\sigma_{Y_i} A_i) \tag{1}$$

$$CoP_{Xseg} = \frac{\Sigma(X_i F_{Zi})}{\Sigma F_{Zi}} \quad CoP_{Yseg} = \frac{\Sigma(Y_i F_{Zi})}{\Sigma F_{Zi}} \tag{2}$$

$$M_{seg} = \Sigma(R_{CoPi} \times F_{AP/MLi}) \tag{3}$$

In addition to net forces, shear forces were also calculated directionally, i.e., all anterior forces were summed separately from posterior forces (Eq. 4).

$$+F_{X,Yseg} = \Sigma(+\sigma_{X,Yi} A_i) \text{ and } -F_{X,Yseg} = \Sigma(-\sigma_{X,Yi} A_i) \tag{4}$$

Modeling and Inverse Dynamics

MSF modeling and inverse dynamics calculations were performed in Visual 3D software (C-Motion, inc. Germantown MD USA) by importing and combining motion capture and segment GRF data. The model was created from a static pose and applied to all walking trials. Dynamic motion data were low pass filtered (6 Hz dual pass Butterworth filter). GRF signals were assigned to their corresponding segments and inverse dynamics calculated.

Data Reporting

Several waveforms and metrics were generated to display segmental forces (and opposing whole foot forces), segmental CoPs, and foot joint kinetics for this normative dataset.

All kinetic metrics were normalized to body weight for presentation.

Net segmental vertical forces and directional AP and ML forces were presented as group ensemble mean waveforms across time-normalized stance phase. Waveforms were time-normalized, averaged across trials and then across participants. Segment impulses (area under the force-time curve) were also calculated to metrically compare the contributions of each segment to the overall impulses. For the AP and ML shear forces, in addition to segment forces, positive and negative shear forces were also summed across the whole foot, and plotted in a similar manner for a simpler visualization of whole foot opposing shear forces. In addition, a novel Pedotti diagram was created for one representative participant to better visualize the interaction between segmental force vectors and their respective CoPs. For this plot, the segment vertical and AP force vectors were plotted against CoP location, while the composite pressure footprint was aligned below it.

To quantify the location and movement of the segment CoPs, weighted averages and weighted standard deviations (in both AP and ML directions) were calculated, weighted across time with a threshold of 10 N for all segments. CoP locations were then normalized to segment length (AP) or segment width (ML) prior to calculating means across subjects.

Internal moments and powers for the ankle, midtarsal, 1MTP, and 23MTP joints were also plotted as group ensemble mean waveforms across time-normalized stance phase. Positive and negative work metrics (integral of power) for each joint were also calculated.

Results

Automated Masking

The masking technique appeared to be successful for all footprints, easily identifying the geometric boundaries dividing the forefoot, hallux, and lateral toes segments (Fig. 3). The linear anatomical boundary between rearfoot and forefoot also appeared to be an appropriate division based on the visual pressure distributions.

Plantar GRFs

Net Segment GRFs

Vertical force data can be found elsewhere [27, 28], but is included here for context with our model (Fig. 4A). The rearfoot segment accounted for 33% (32.6 ± 5.0 %) of the total vertical impulse, the forefoot 52% (52.5 ± 4.8 %), the hallux 12% (12.2 ± 3.4 %), and lateral toes 3% (2.7 ± 1.7 %).

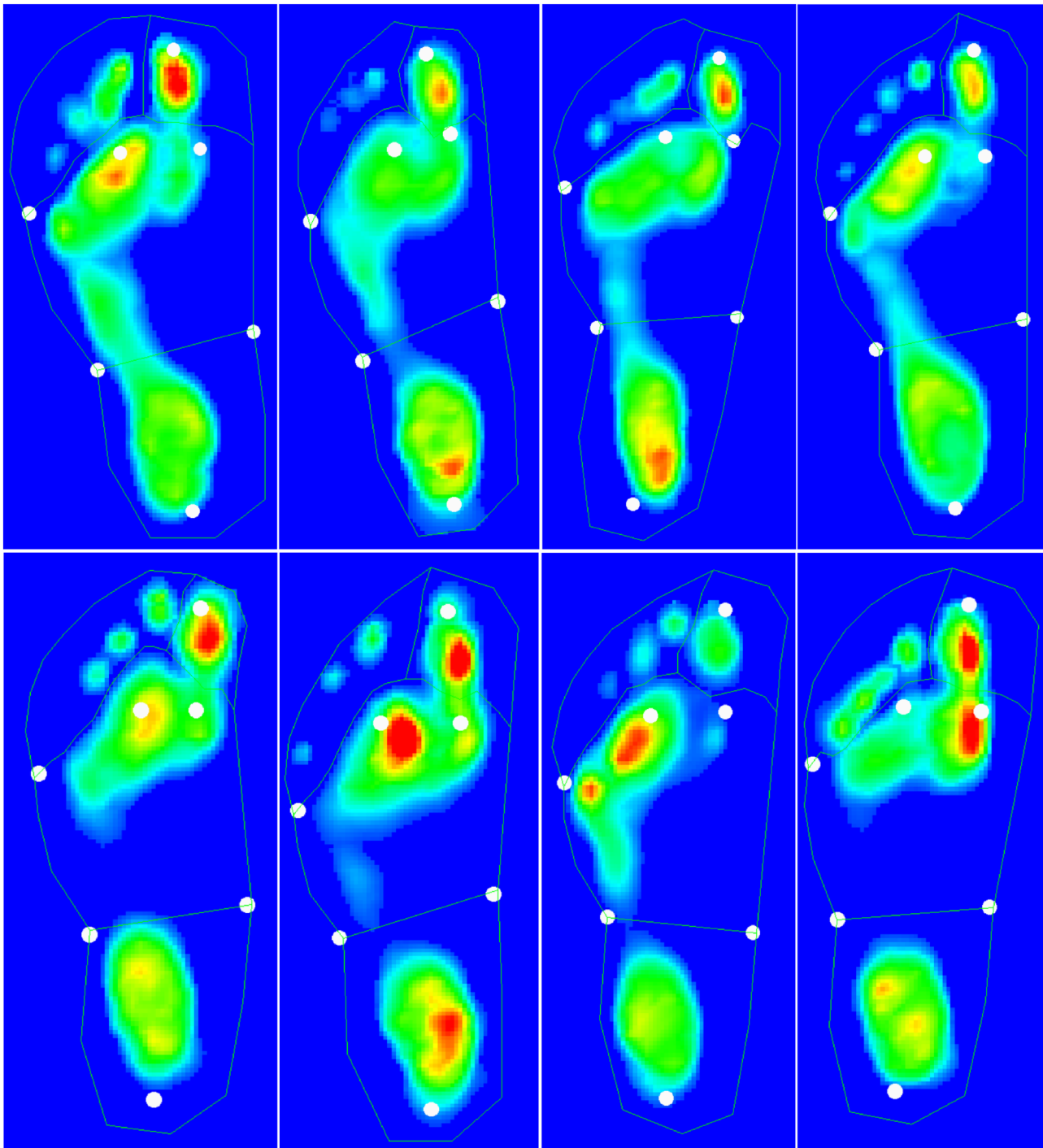


Fig. 3 Footprint masking results, illustrating the effectiveness of the method on a variety of footprints. White circles represent markers used in the masking process, with lines outlining the segment boundaries

From a timing standpoint, the forefoot was engaged throughout most of stance, with just a brief unloaded period at the beginning (5%) and end (2%) of stance. The hallux engaged at about 30% of stance, with the lateral toes engaging much later (55% of stance), approximately at the same time as the heel completed unloading.

For AP forces (Fig. 4B), the net braking (posterior) force was dominated by the rearfoot, with a small contribution from the forefoot. Propulsive (anterior) forces arose primarily from the forefoot, with small contributions from the hallux and lateral toes. The hallux also applied a notable braking impulse in terminal stance prior to transitioning to

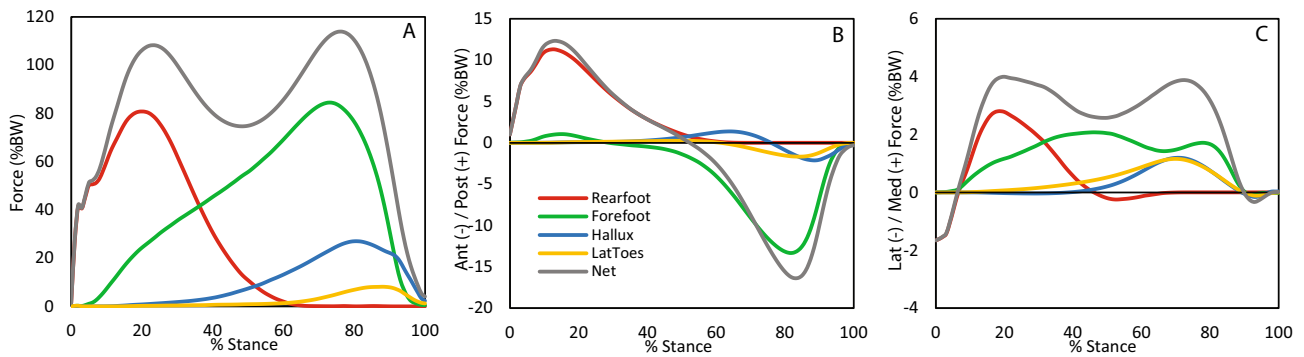


Fig. 4 Ensemble mean segment GRFs across time-normalized stance phase. **A** Vertical force, **B** AP shear force, **C** ML shear force

propulsion. For ML forces (Fig. 4C), All segments exhibited a substantial net medial force, with only small lateral forces at the beginning or end of each segment’s engagement.

Segment CoP

The CoP under each segment showed relatively little movement across stance, with a mean weighted standard deviation ranging from just 1.0 mm (Hallux ML) up to 8.2 mm (Forefoot AP) (Table 1). The mean weighted location of the COP in the AP direction was just under half the length of the rearfoot (44%), the forefoot was further distal (78%), while the hallux and lateral toes were just over half their length (62%). In the ML direction, the COP was located just lateral to the long axis of each segment; ranging from 3.2 mm lateral for the Hallux up to 4.5 mm for the lateral toes. Segmental CoP locations and associated net GRF vectors (vertical and ML) are visually illustrated by the segmental butterfly diagram for a representative participant (Fig. 5).

Directional Shear Forces

Separating positive and negative directional shear forces across the whole foot, there were opposing AP forces

between the two main AP peaks (braking and propulsive), approximately 15% to 85% of stance (Fig. 6A). The greatest opposition occurred in mid-stance, with equal positive and negative forces of about 4% BW, roughly 25–30% of the peak braking and propulsive forces. Opposing shear forces in the ML direction were consistent across stance, with an opposing lateral force of about 2.5% BW, or about 40% of the average medial force (Fig. 6D).

When AP forces were broken out by both direction and segment, the rearfoot force proved almost entirely unidirectional, creating the main posterior braking impulse (Fig. 6B). The forefoot GRF was primarily directed anteriorly, but also contained some small opposing posterior forces within the segment through most of early and mid-stance. Matching vertical forces, the forefoot engaged with the ground early in stance, however, early stance shear forces mostly canceled each other out, resulting in smaller net force until mid-stance. These within-segment opposing shear forces appeared to be primarily located under the metatarsal heads (see also CoP results). For a brief period in mid-stance (40–50%), there were also opposing forces between the rearfoot and forefoot, presumably as the medial longitudinal arch (MLA) dropped just prior to heel off. In late stance, the forefoot eventually transitioned to

Table 1: Location of segment CoPs

	Rearfoot	Forefoot	Hallux	Lat. Toes
Seg length (cm)	9.25 ± 0.66	10.82 ± 0.90	5.37 ± 0.61	5.37 ± 0.61
Seg width (cm)	7.39 ± 0.7	8.45 ± 0.9	2.00 ± 0.0	8.45 ± 0.9
AP mean (%)	44.2 ± 5.2 %	78.5 ± 5.9 %	61.9 ± 8.9 %	61.9 ± 16.6 %
AP SD (%)	4.6 ± 1.5 %	7.5 ± 4.1 %	4.4 ± 1.3 %	7.3 ± 2.4 %
ML mean (%)	- 5.4 ± 4.8 %	- 3.6 ± 6.2 %	- 15.8 ± 11.5 %	- 5.3 ± 10.6 %
ML SD (%)	1.8 ± 0.8 %	5.9 ± 2.2 %	5.1 ± 2.2 %	5.3 ± 1.7 %

Group means for the weighted mean location and weighted standard deviation of location are presented as percentages of segment length or width, which are also displayed. Segment lengths were taken from the model (i.e., long axis length), with the lateral toes matched to the hallux. Widths were also derived from the model markers: rearfoot width between navicular and cuboid markers, forefoot and lateral toes width between 1st and 5th metatarsal head markers, and hallux assigned a fixed width of 2 cm

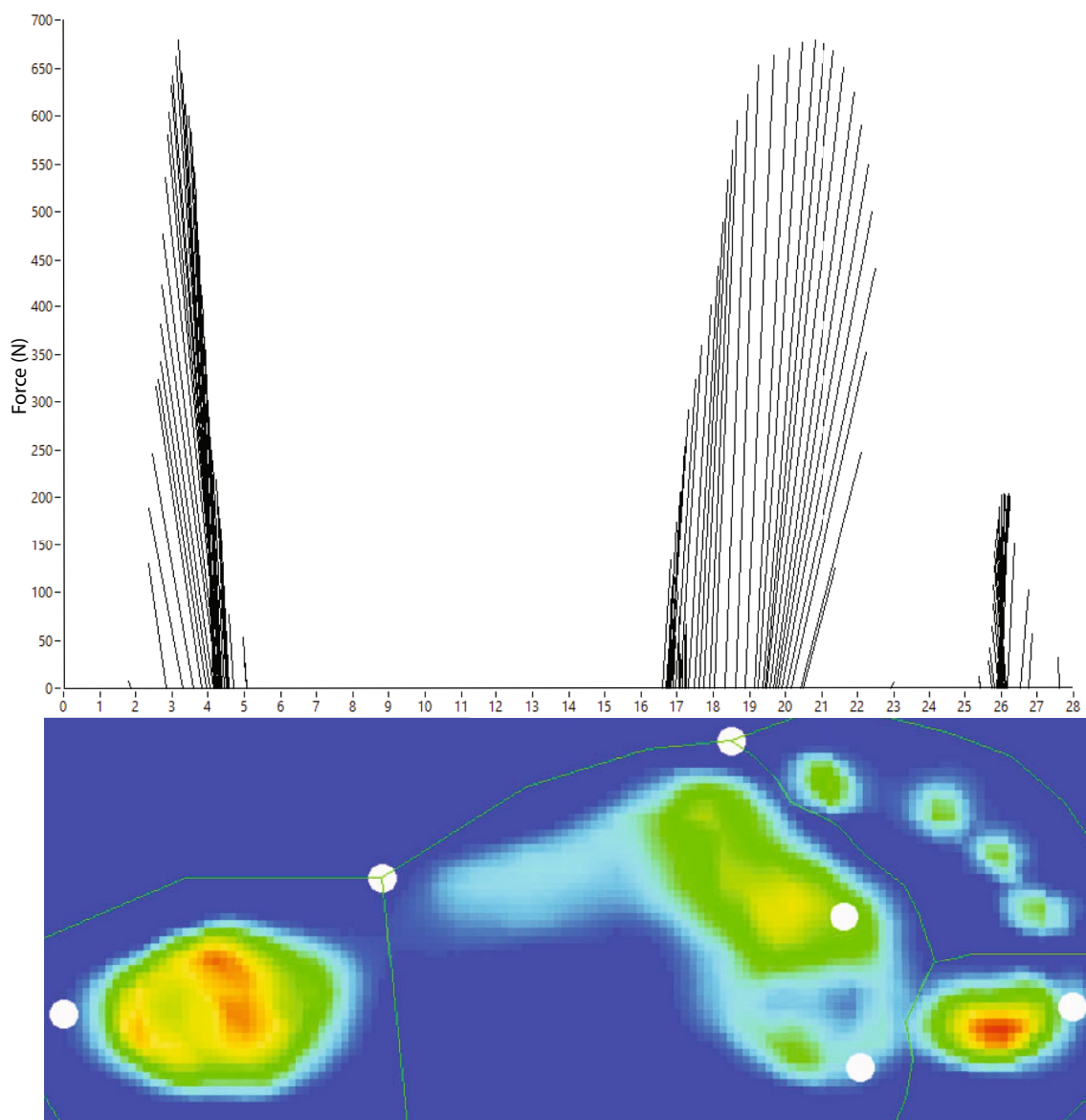


Fig. 5 Multi-segment foot Pedotti or butterfly diagram for one representative participant ($h=176$ cm, $m=75$ kg). The composite pressure image is spatially aligned with the horizontal axis of the butterfly

diagram (in cm). For clarity the hallux forces are shown but not the lateral toes (because they are near the same location)

a unidirectional propulsive force. The hallux also showed some brief within-segment opposing forces only as it transitioned from braking to propulsive. The lateral toes, on the other hand, were almost entirely propulsive, roughly equaling the propulsive impulse of the hallux (Fig. 6C). By percentage, the rearfoot had an opposing anterior impulse of just 5% of its primary posterior impulse; the forefoot had a posterior impulse of 20% of its primary anterior impulse; the hallux was more split, with a slightly greater posterior impulse than anterior impulse (90% of posterior); the LatToes had a posterior impulse that was just 10% of its primary anterior impulse.

ML directional shear forces showed opposing shear forces in all segments, although the lateral toes had very little lateral forces (Fig. 6E). The three other segments all contributed an opposing impulse between 20 and 30% of their primary impulses (Fig. 6F).

Joint Kinetics

Joint moments in each plane (Figure 7A–C) showed comparatively little contribution from the 2-3MTP joint, thus this was excluded from the descriptions that follow. In the sagittal plane (Fig. 7A), the ankle displayed a small initial

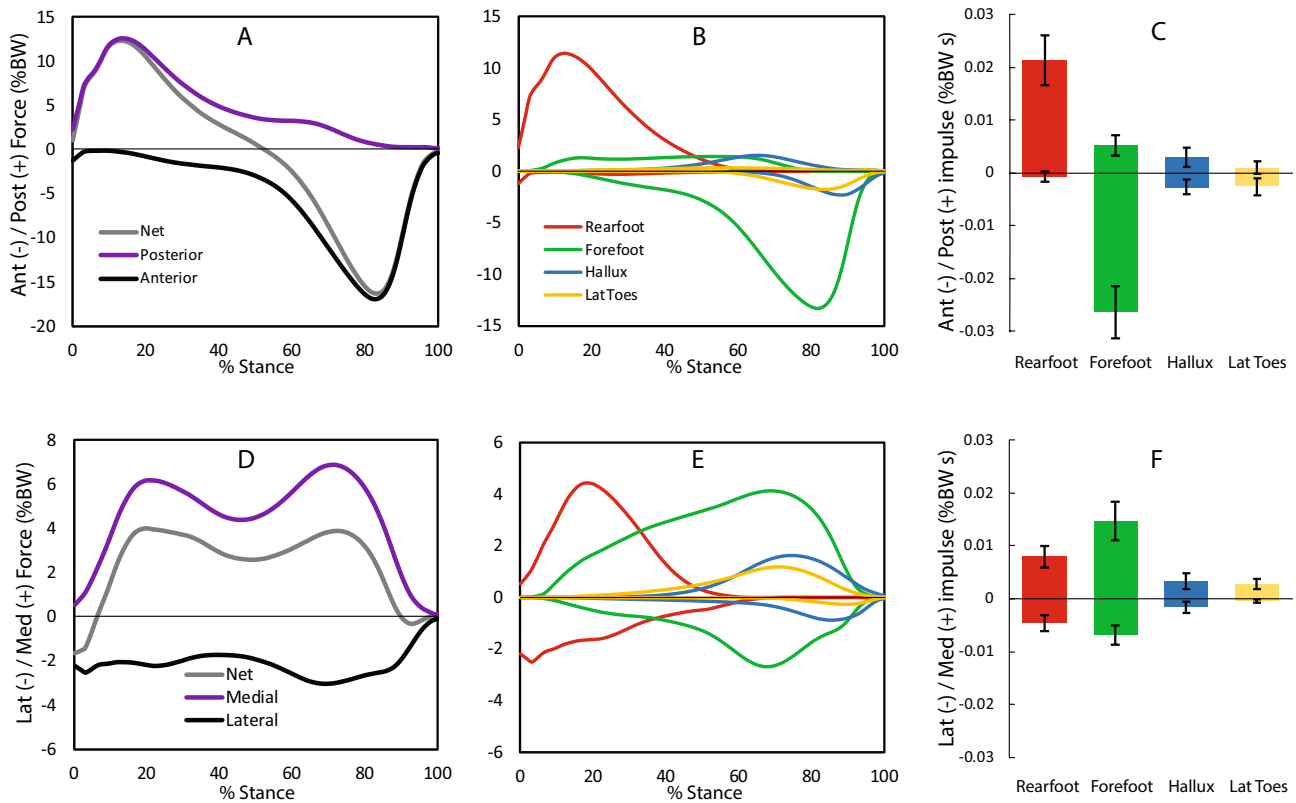


Fig. 6 Ensemble mean directional shear forces, plotted across time-normalized stance phase (A–E), and associated impulse values for each segment (C–F). Directional forces were plotted as net forces for

the whole foot (A, D) as well as broken out by segment (B, E). Top row of plots represents AP directions (A–C) while the bottom row represents ML directions (D–F)

dorsiflexion moment in early stance (peak 0.11 N/kg), transitioning to a plantarflexion moment around 20% and peaking (1.44 N/kg) around 75% of stance. The midtarsal joint only exhibited a plantarflexion moment, starting at 5% stance and peaking (1.16 N/kg) around 78% of stance. The 1MTP exhibited a much smaller plantarflexion moment (peak 0.09 N/kg), notable only after 60% of stance. In the frontal plane (Fig. 7B), the ankle had an inversion moment (peak 0.05 N/kg) during the first half of stance followed by a larger eversion moment (peak 0.23 N/kg) for the remainder of stance. The midtarsal joint had an inversion moment through most of stance (peak 0.12 N/kg), transitioning to a small eversion moment only for the last 15% of stance (peak 0.04 N/kg). The 1MTP joint exhibited a small inversion moment only during the final 20% of stance (peak 0.01 N/kg). In the transverse plane (Fig. 7C), there was an external rotation moment at the ankle from 20 to 100% of stance (peak 0.13 N/kg) and a smaller opposing internal rotation moment at the midtarsal joint from 40 to 90% (peak 0.01 N/kg). The midtarsal and 1MTP joints had opposing moments for the final 10% of stance, external at the midtarsal (peak 0.01 N/kg) and internal at the 1MTP (peak 0.01 N/kg).

Ankle and midtarsal joint power waveforms showed similar transitions from negative to positive power, at about 75% of stance (Fig. 7D). Negative work done by the ankle was nearly double the work done by the midtarsal joint, however positive work done was nearly equal (Fig. 7E). Both the 1MTP and 23MTP joints primarily absorbed power, with the 1MTP joint performing similar negative work to the midtarsal joint, while the 23MTP joint absorbed about 20% of that amount. Peak energy absorption at both MTP joints occurred roughly concurrently with peak energy generation at the ankle and midtarsal joints.

Discussion

This study focused on the development of methodology to integrate pressure/shear stress measurements with MSF modeling and on the display of normative measures of data generated during healthy gait. Discussion below is organized around our three main hypotheses, covering automated masking, presentation of segmental directional forces, and interpretation of joint kinetics.

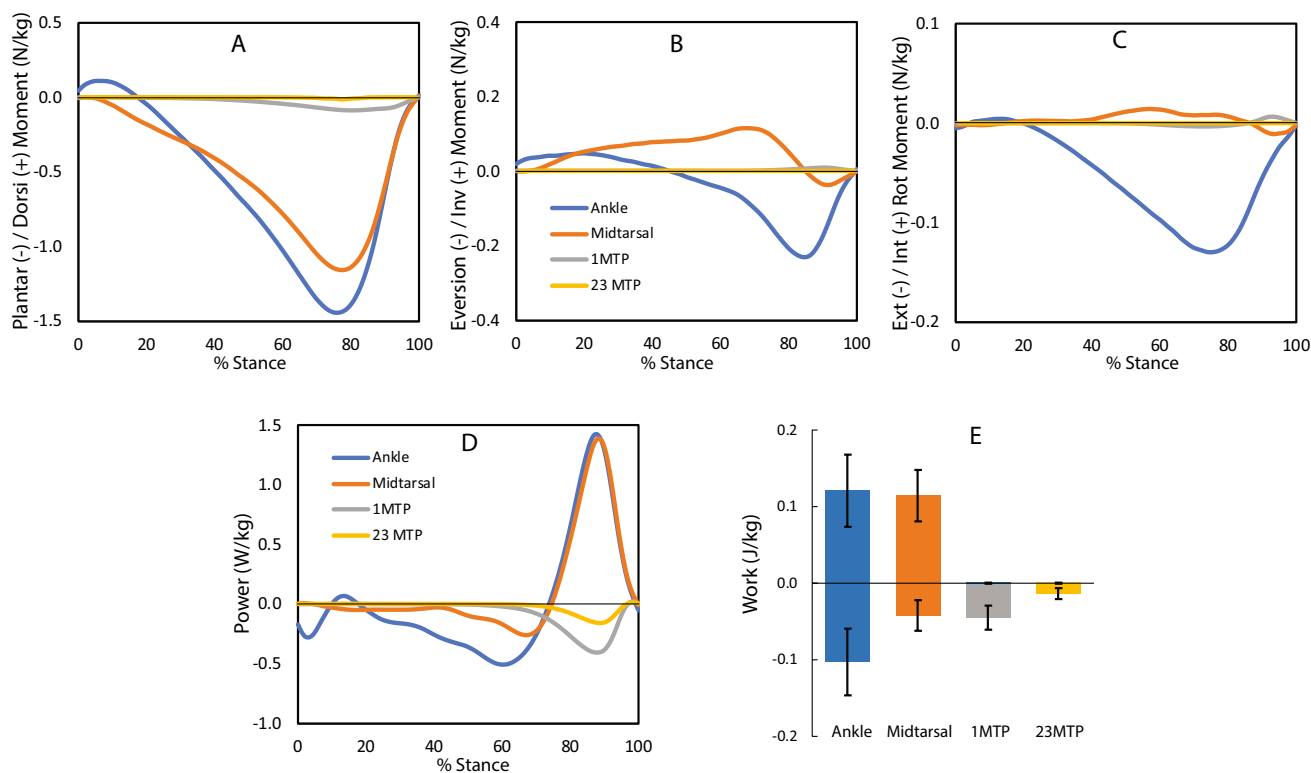


Fig. 7 Internal joint moments and joint power for the ankle, midtarsal, 1MPT, and 23MTP joints. The top row of graphs (A–C) represents joint moments in each proximal segment’s sagittal (A), frontal (B), and transverse (C) planes. The bottom row (D, E) represent

scalar joint power (D) and associated work values (integral of power, separated positive and negative) (E). All time series graphs (A–D) are displayed across time-normalized stance

Automated Masking

Aligning masking with multi-segment foot modeling brings a functional perspective to the masking process. While masking of composite pressure footprints has been performed in various capacities for decades, there is no consensus on an ideal number of ROIs nor their identification criteria [16]. One reason for this is that the primary motivation behind masking is simply the extraction of pressure metrics [16]. Coupling masking with a multi-segment foot model expands this focus from isolated plantar tissues to broader foot function. For instance, many forefoot ROIs span both the metatarsal heads and phalanges [17, 18, 20], presumably for ease of identification; however, the metatarsophalangeal joints provide a critical division when analyzing foot joint mechanics. Conversely, the rearfoot is often split into ML regions [15, 16, 18, 20]; however, the bony rearfoot segment (i.e., calcaneus) is a rigid body [26] with a fairly confined center of pressure, as shown in this paper. While other models are certainly possible, our four segment model represents a starting point for functional alignment of foot tissues with joint mechanics.

Our masking definitions, while motivated by foot articulations from our model, were also aligned with some

geometric considerations. The midtarsal joint center was defined solely by marker locations, but it appeared to also delineate the visual geometric division between rearfoot and forefoot ROIs in our healthy sample. In pathological gait, a purely geometric division in this region is likely to contain substantially higher variability than an anatomical one due to deformities [18]. Note also that an additional midfoot segment with a distal joint between the cuneiforms and metatarsals has been proposed in other modeling work [10]—this ROI division is definitely possible using anatomical landmarks, but does not appear to have any clear geometric pressure boundaries. Between the forefoot and phalanges segments (hallux or lateral toes), there is some pressure data just distal to the MTP joint centers from plantar tissues that extend anterior to the metatarsal heads. We chose to attribute these tissues to the forefoot segment for two reasons: (1) these tissues surround the larger metatarsal heads, thus force transmission is likely applied to the forefoot segment and not the phalanges, and (2) there is a clear geometric boundary just distal to them, similar to what has been done with some proprietary commercial geometric masking techniques [29].

The presented template masking process is versatile and could be adapted to other models and study populations. Previous attempts at integrating pressure with motion capture

have primarily relied on purely anatomical masking [10, 17–20] or on manual masking [3, 9, 11]. For the former, the forefoot and phalanges have either been combined [17, 18, 20] or the boundary between them identified by a straight line between markers [10, 19], which may overestimate the distal forces. Manual masking can certainly be useful for small research studies, but is obviously cumbersome for larger studies and clinical practice [30]. Due to the use of a template, our combined anatomical and geometric approach can be both automated and customized. Although we used only healthy participants, the template approach could in theory be customized to any sub-group, including challenging foot pathologies such as clubfoot [18, 30].

Segmental Directional Forces

While some of the force analysis presented in this paper could also be performed without a matching MSF model (e.g., net directional shear forces), the model provides context and insights. For instance, our analysis shows relatively stationary segmental CoPs, contrasting with the typical whole foot approach focusing on the forward progression of the CoP [31]. Our initial hypothesis was based on Segal et al. [32], who also reported similar findings in supplemental material, but did not discuss them. These results suggest that forward CoP progression arises more from changes in force weighting between segments as opposed to CoP movement within a segment. In other words, whole foot AP CoP progression arises primarily from redistributing weight across fairly fixed segmental contact points. This new perspective could influence tenets such as the center of pressure velocity and roll-over shape commonly used in prosthetics [33, 34], dynamic walking models [35], and pathologies [36], and future work in more complex segmental analogs to these models may provide additional insights.

Summed directional shear forces are a concise way to summarize complex shear stress distributions across the foot. In addition to whole time series waveforms, extracted metrics may also be useful, including impulses (presented here) or opposing shear at specific time points [13, 24]. For the latter, our normative data suggests that AP opposing forces peak in mid-stance at the (net) zero crossing, and a metric at this point may best capture opposing AP shear [24]. ML opposing forces are more consistent across time and a mean value could be extracted. Expanded butterfly diagrams like ours or Berki et al. [37] are useful visualization tools, although not practical for group analyses. The presented vertical and AP diagram (Figure 5) displays the CoP concentrations as well as the segmental AP shear directions. An ML version of this diagram could also be created, but is more challenging. Stucke et al. [14] previously evaluated directional shear forces in the context of diabetes, referring to areas of primarily unidirectional shear as “dragging”, and

substantial bidirectional (opposing) shear as “spreading.” This terminology may be useful and we suggest adopting it and expanding its use to describe both within and between segment directional shear forces.

AP shear forces are related to locomotion energetics, as posterior dragging forces are expected during the braking impulse, and anterior dragging forces during the propulsive impulse. However, there were some instances of spreading, suggesting energy dissipation and potential areas of inefficiencies when excessive. This spreading occurred both between and within segments. There was some spreading between the rearfoot and forefoot, presumably as the midtarsal joint dorsiflexes (i.e., MLA drop) and begins performing negative work. There was also some spreading within the forefoot which was not due to foot joint motion (primarily soft tissue deformation in the area around the metatarsal heads). Similarly, there was a small amount of spreading between the forefoot and hallux that accompanied negative MTP joint work, and some spreading within the hallux segment itself. The data presented in this study provide baseline values that may be leveraged when looking at gait inefficiencies or balance impairments that might occur with pathology.

ML spreading occurred throughout stance and within all segments. In the more rigid rearfoot and hallux segments, this suggests skin spreading independent from joint motion. In the forefoot, some of this may also represent motion among the multiple joints contained in the single segment. While this is certainly possible for a kinematic only model, it is difficult to further segment the forefoot for a kinetic model as ML forces between metatarsals cannot easily be resolved using traditional inverse dynamics [38]; thus the reason for a single forefoot segment in our model. The ML shear measurements, however, could be useful in investigating the controversial transverse arch [15, 39]. ML spreading may also be useful in dynamic stability and should be further studied from a balance and proprioception perspective [24]. In addition, spreading that is slightly offset from the CoP contributes to the free moment, and additional exploration into segmental contributions to this moment may be useful [40].

Joint Kinetics

While a number of kinetic multi-segment foot modeling papers have been published [1–3, 10, 11], the complexity of data collection and interpretation has prevented their widespread adoption and clinical implementation. Joint powers have been the most useful, and have influenced our view of foot energetics; for instance, modifying the long-held tenet that the ankle is the primary driver of propulsive energy [41], as substantial mechanical work appears to be attributable to the foot itself [42]. Yet, the sources of this positive

work are not clear. Our scalar power results visually match these previous estimates but overcome some errors due to force distribution assumptions [7]. In addition, we add to the body of literature on this topic by separating the contribution of the hallux and lateral toes, noting that there was about a 5:1 ratio of negative work done by the 1MTP to 23MTP joints.

Despite normative foot joint moment values having been published for over two decades [43], use of non-sagittal plane moments has gained little traction in either research or clinical practice, similar to non-sagittal plane ankle moments. A major reason for this is interpretation difficulty. While net moments about larger, more mobile joints can be mostly attributed to active muscle contributions, the complexity of the foot joint structures makes it difficult to separate the contributions of muscles, tendons, ligaments, or other connective tissues. We suggest a few perspectives that may increase non-sagittal moment utility below, but propose combining the measurement methods used in the current study with detailed musculoskeletal modeling [44] to help isolate individual tissue contributions.

Since inertial effects are extremely small in the foot [1], moments are almost entirely composed of the GRF and its lever arm, represented by the location of the CoP relative to the joint center. Recognizing the fairly stationary nature of segment CoPs may help in visualizing joint moments, particularly in late stance. For instance, in the frontal plane, the CoP for each segment was primarily positioned just lateral to each joint line, resulting in internal inversion moments at most joints. These moments may be better described as medial foot tissue stress, resulting from some combination of muscle contractions or passive tissue tension. The ankle is slightly more complex to visualize in this way, with the moment transitioning from inversion to eversion (or lateral tissue stress) in mid-stance, but should also be interpreted in terms of stress instead of muscle actions. Transverse plane moments may be closely linked to free moments, and, again, additional analysis connecting opposing shear with these moments may be helpful. Non-sagittal plane moments have begun to contribute to our understanding of gait, for instance in ankle instability [45] and uneven surface adaptations [32], and coupled with other measurement and modeling techniques could expand their usefulness.

Challenges

Early integration of these devices is not without methodology challenges. Capturing pressure and shear distributions leads to data handling challenges from large data files (~500 MB per trial) and substantial initial processing time (~20 min per trial). The pressure/shear capture resolution (2.12 mm²) and sampling rate (50 Hz) are driven by the sensor's camera, which can be increased at the cost of

additional data handling. In this application, it may actually be desirable to reduce camera resolution in order to increase sampling rate, since segmental GRFs require only sufficient resolution to create accurate segment masks. Currently, processing time may limit certain applications (e.g., clinical setting), with the most time intensive step being the reconstruction model of applied forces from film images during initial processing. This is due to very dense meshes used in the finite element model. Future studies will be directed at determining how much both the sensor resolution and finite element mesh resolution can be reduced while maintaining good quality force data. Alternatively, since we only used the reconstructed pressure data (and raw shear data), other experimental approaches that don't require finite element reconstruction will also be investigated.

Acknowledgements We would like to thank Kade Scoresby, Jordan Grover, Jared Staten, Kirk Bassett, Lauren Williams, and Hwigeum Jeong for their help with data collection. KB and LW also assisted with data analysis. We would also like to thank Barb Cutler for her help with the masking algorithm.

Declarations

Conflict of interest No conflicts of interest to declare

References

1. Bruening, D. A., K. M. Cooney, and F. L. Buczek. Analysis of a kinetic multi-segment foot model part II: kinetics and clinical implications. *Gait Posture*. 35(4):535–540, 2012.
2. Dixon, P. C., H. Böhm, and L. Döderlein. Ankle and midfoot kinetics during normal gait: a multi-segment approach. *J. Biomech.* 45(6):1011–1016, 2012.
3. MacWilliams, B. A., M. Cowley, and D. E. Nicholson. Foot kinematics and kinetics during adolescent gait. *Gait Posture*. 17(3):214–224, 2003.
4. Scott, S. H., and D. A. Winter. Biomechanical model of the human foot: kinematics and kinetics during the stance phase of walking. *J. Biomech.* 26(9):1091–1104, 1993.
5. Leardini, A., P. Caravaggi, T. Theologis, and J. Stebbins. Multi-segment foot models and their use in clinical populations. *Gait Posture*. 69:50–59, 2019.
6. Bruening, D. A., K. M. Cooney, F. L. Buczek, and J. G. Richards. Measured and estimated ground reaction forces for multi-segment foot models. *J. Biomech.* 43(16):3222–3226, 2010.
7. Bruening, D. A., and K. Z. Takahashi. Partitioning ground reaction forces for multi-segment foot joint kinetics. *Gait Posture*. 62:111–116, 2018.
8. Stefanyshyn, D. J., and B. M. Nigg. Mechanical energy contribution of the metatarsophalangeal joint to running and sprinting. *J. Biomech.* 30(11–12):1081–1085, 1997.
9. Giacomozzi, C., and V. Macellari. Piezo-dynamometric platform for a more complete analysis of foot-to-floor interaction. *IEEE Trans. Rehabil. Eng.* 5(4):322–330, 1997.
10. Deschamps, K., M. Eerdeken, D. Desmet, G. A. Matricali, S. Wuite, and F. Staes. Estimation of foot joint kinetics in three and four segment foot models using an existing proportionality scheme: application in paediatric barefoot walking. *J. Biomech.* 61:168–175, 2017.

11. Saraswat, P., B. A. MacWilliams, R. B. Davis, and J. L. D'Astous. Kinematics and kinetics of normal and planovalgus feet during walking. *Gait & Posture*. 39(1):339–345, 2014.
12. Goss, L. P., J. W. Crafton, B. L. Davis, et al. Plantar pressure and shear measurement using surface stress-sensitive film. *Meas. Sci. Technol.* 31(2):025701, 2019.
13. Davis, B., M. Crow, V. Berki, and D. Ciltea. Shear and pressure under the first ray in neuropathic diabetic patients: implications for support of the longitudinal arch. *J. Biomech.* 52:176–178, 2017.
14. Stucke, S., D. McFarland, L. Goss, et al. Spatial relationships between shearing stresses and pressure on the plantar skin surface during gait. *J. Biomech.* 45(3):619–622, 2012.
15. Cavanagh, P. R., M. M. Rodgers, and A. Liboshi. Pressure distribution under symptom-free feet during barefoot standing. *Foot Ankle*. 7(5):262–278, 1987.
16. Deschamps, K., P. Roosen, F. Nobels, et al. Review of clinical approaches and diagnostic quantities used in pedobarographic measurements. *J. Sports Med. Phys. Fitness*. 55(3):191–204, 2015.
17. Giacomozzi, C., M. G. Benedetti, A. Leardini, V. Macellari, and S. Giannini. Gait analysis with an integrated system for functional assessment of talocalcaneal coalition. *J. Am. Podiatric Med. Assoc.* 96(2):107–115, 2006.
18. Giacomozzi, C., and J. A. Stebbins. Anatomical masking of pressure footprints based on the Oxford Foot Model: validation and clinical relevance. *Gait Posture*. 53:131–138, 2017.
19. Sawacha, Z., G. Guarneri, G. Cristoferi, A. Guiotto, A. Avogaro, and C. Cobelli. Integrated kinematics–kinetics–plantar pressure data analysis: a useful tool for characterizing diabetic foot biomechanics. *Gait Posture*. 36(1):20–26, 2012.
20. Stebbins, J., M. Harrington, C. Giacomozzi, N. Thompson, A. Zavatsky, and T. Theologis. Assessment of sub-division of plantar pressure measurement in children. *Gait Posture*. 22(4):372–376, 2005.
21. Perry, J., and J. M. Burnfield. *Gait Analysis. Normal and Pathological Function*, 2nd ed. California: Slack, 2010.
22. McMulkin, M. L., and B. A. MacWilliams. Application of the gilette gait index, gait deviation index and gait profile score to multiple clinical pediatric populations. *Gait Posture*. 41(2):608–612, 2015.
23. Pataky, T. C. Generalized n-dimensional biomechanical field analysis using statistical parametric mapping. *J. Biomech.* 43(10):1976–1982, 2010.
24. Jeong, H., A. W. Johnson, J. B. Feland, S. R. Petersen, J. M. Staten, and D. A. Bruening. Added body mass alters plantar shear stresses, postural control, and gait kinetics: implications for obesity. *PLoS ONE*. 16(2):e0246605, 2021.
25. Williams, L. R., S. T. Ridge, A. W. Johnson, E. S. Arch, and D. A. Bruening. The influence of the windlass mechanism on kinematic and kinetic foot joint coupling. *J. Foot Ankle Res.* 15(1):1–11, 2022.
26. Bruening, D. A., K. M. Cooney, and F. L. Buczek. Analysis of a kinetic multi-segment foot model. Part I: model repeatability and kinematic validity. *Gait Posture*. 35(4):529–534, 2012.
27. Hutton, W., and M. Dhanendran. The mechanics of normal and hallux valgus feet—a quantitative study. *Clin. Orthop. Relat. Res.* 157:7–13, 1981.
28. Wearing, S., S. Urry, and J. Smeathers. Ground reaction forces at discrete sites of the foot derived from pressure plate measurements. *Foot Ankle Int.* 22(8):653–661, 2001.
29. Ellis, S. J., H. Stoecklein, J. C. Yu, G. Syrkin, H. Hillstrom, and J. T. Deland. The accuracy of an automasking algorithm in plantar pressure measurements. *HSS J.* 7(1):57–63, 2011.
30. Wallace, J., H. White, S. Augsburger, and J. Walker. Development of a method to produce a valid and reliable foot mask for plantar pressure evaluation in children with clubfoot. *J. Pediatric Orthop. B.* 30(3):287–295, 2021.
31. Jameson, E. G., J. R. Davids, J. P. Anderson, R. B. Davis III., D. W. Blackhurst, and L. M. Christopher. Dynamic pedobarography for children: use of the center of pressure progression. *J. Pediatric Orthop.* 28(2):254–258, 2008.
32. Segal, A. D., K. H. Yeates, R. R. Neptune, and G. K. Klute. Foot and ankle joint biomechanical adaptations to an unpredictable coronally uneven surface. *J. Biomech. Eng.* 140(3):031004, 2018.
33. Hansen, A. H., M. Meier, M. Sam, D. Childress, and M. Edwards. Alignment of trans-tibial prostheses based on roll-over shape principles. *Prosthet. Orthot. Int.* 27(2):89–99, 2003.
34. Klenow, T. D., J. T. Kahle, and M. J. Highsmith. The dead spot phenomenon in prosthetic gait: quantified with an analysis of center of pressure progression and its velocity in the sagittal plane. *Clin. Biomechan.* 38:56–62, 2016.
35. Adamczyk, P. G., S. H. Collins, and A. D. Kuo. The advantages of a rolling foot in human walking. *J. Exp. Biol.* 209(20):3953–3963, 2006.
36. Li, B., Q. Xiang, and X. Zhang. The center of pressure progression characterizes the dynamic function of high-arched feet during walking. *J. Leather Sci. Eng.* 2(1):1–10, 2020.
37. Berki, V., M. A. Boswell, D. Ciltea, et al. Expanded butterfly plots: a new method to analyze simultaneous pressure and shear on the plantar skin surface during gait. *J. Biomech.* 48(10):2214–2216, 2015.
38. Buczek, F. L., M. R. Walker, M. J. Rainbow, K. M. Cooney, and J. O. Sanders. Impact of mediolateral segmentation on a multi-segment foot model. *Gait Posture*. 23(4):519–522, 2006.
39. Venkadesan, M., A. Yawar, C. M. Eng, et al. Stiffness of the human foot and evolution of the transverse arch. *Nature*. 579(7797):97–100, 2020.
40. Ohkawa, T., T. Atomi, M. Shimizu, and Y. Atomi. Relationship of lower extremity kinematics in the sagittal plane with free moment during walking. *J. Fiber Sci. Technol.* 77(10):250–257, 2021.
41. Winter, D. A. Energy generation and absorption at the ankle and knee during fast, natural, and slow cadences. *Clin. Orthop. Relat. Res.* 175:147–154, 1983.
42. Zelik, K. E., and E. C. Honert. Ankle and foot power in gait analysis: implications for science, technology and clinical assessment. *J. Biomech.* 75:1–12, 2018.
43. Hunt, A. E., R. M. Smith, and M. Torode. Extrinsic muscle activity, foot motion and ankle joint moments during the stance phase of walking. *Foot Ankle Int.* 22(1):31–41, 2001.
44. Malaquias, T. M., C. Silveira, W. Aerts, et al. Extended foot-ankle musculoskeletal models for application in movement analysis. *Comput. Methods Biomech. Biomed. Eng.* 20(2):153–159, 2017.
45. Moisan, G., C. Mainville, M. Descarreaux, and V. Cantin. Lower limb biomechanics in individuals with chronic ankle instability during gait: a case-control study. *J. Foot Ankle Res.* 14(1):1–9, 2021.

Publisher's Note Springer Nature remains neutral with regard to jurisdictional claims in published maps and institutional affiliations.

Springer Nature or its licensor (e.g. a society or other partner) holds exclusive rights to this article under a publishing agreement with the author(s) or other rightsholder(s); author self-archiving of the accepted manuscript version of this article is solely governed by the terms of such publishing agreement and applicable law.